RECLAMATION
Managing Water in the West

Technical Memorandum No. EVMAA-8668460-2008-1

El Vado Dam Middle Rio Grande Project, New Mexico

Issue Evaluation — Service Spillway – Operational Testing & Dynamic Analysis

U.S. Department of the Interior
Bureau of Reclamation
Technical Service Center
Hydraulic Investigations and Laboratory Services
Denver, Colorado

August 2008

BUREAU OF RECLAMATION
Technical Service Center, Denver, Colorado
Hydraulic Investigations and Laboratory Services Group, 86-68460

Technical Memorandum No. EVMAA-8668460-2008-1

El Vado Dam Middle Rio Grande Project, New Mexico

Issue Evaluation — Service Spillway – Operational Testing & Dynamic Analysis

Prepared: K. Warren Frizell
Research Hydraulic Engineer, 86-68460

Checked: Joseph P. Kubitschek, P.E.
Hydraulic Engineer, 86-68460

Peer Review: Robert V. Todd, P.E.
Consulting Mechanical Engineer, EGS, Inc.

9-4-2008
Date

Background

El Vado Dam located on the Rio Chama about 160 miles north of Albuquerque, was built by the Middle Rio Grande Conservancy District in 1934-1935 and was rehabilitated by the Bureau of Reclamation in 1954-1955. A new outlet works was built by Reclamation in 1965-1966 to accommodate the additional water from the San Juan-Chama Project. The dam embankment is of rolled gravel fill with a steel membrane on the upstream face. The dam is 175 feet high and has a crest length of 1,326 feet. The reservoir has a total capacity of 196,500 acre-feet. The service spillway is a steel-plate-lined channel with inflow controlled by a 36-ft by 24-ft radial gate. The spillway channel is located on the right abutment and is founded on earthen material that includes Mancos shale.

The service spillway at El Vado Dam is a unique design, unlike any other structure that Reclamation operates and maintains. Over the years, maintenance activities on the spillway have included weld repairs to cracks and failed welds. These repairs have been only partially successful due to post repair cracking in the heat affected zones of the welds. The floor/invert plates are $^{5}/_{16}$-in-thick and the wall plates are ¼-in-thick; both invert and side wall lining plates are attached to a steel channel support system using 13/16-inch-diameter plug welds.

This technical memorandum will serve as the deliverable for the Operational Testing and Dynamic Analysis of the Service Spillway at El Vado Dam, funded by Reclamation's Dam Safety Office to satisfy SOD recommendation 2006-SOD-A. This report summarizes testing at the dam site during the week of June 23, 2008. The testing included a modal survey of several spillway lining plates and in addition, results from strain and acceleration measurements during an operational test of the spillway. The results of the testing were used to perform a fatigue life analysis and additional structural analyses in order to provide critical input for future risk assessment and associated flood routing decisions.

Field Testing

An initial site visit on June 9-10, 2008 focused on the amount of dewatering effort that would be required in order for our planned testing to occur. The spillway floor plates over the lower one-half end of the spillway and at minimum three-quarters of the channel width must be dry and completely free from the leakage flows. Leakage flow rates were estimated at between 50-100 ft^3/s during this first site visit, figure 1a.

Testing was accomplished during the week of June 23, 2008. Leakage had been reduced and contained to the right side of the spillway allowing access to the areas that required instrument placement and installation, figure 1b. The test plan called for a modal survey of several spillway plates, a review of the data, and then selection and installation of strain gages and accelerometers that would be waterproofed and monitored during the operational tests.

Modal Survey

The modal survey included 3 general locations along the left half of the spillway invert and associated sidewall plates, figure 2. These plates were chosen based partly on their location within the lower half of the spillway channel where velocities will be higher and also on their apparent loss of support beneath the plates, at least in some areas. The modal survey was completed using 7 accelerometers with magnetic mounts and an instrumented force hammer (3 lb) to provide the impulse excitation. Six accelerometer placements were required to document the 24-ft-long floor plates and corresponding side wall plates at locations 1 and 2. At location 3, only two tests were required to document the 8 ft-4 in-long plate and associated side wall plate, figure 3. Figure 4 shows placement of the accelerometers in a grid in preparation for impulse testing. Three different impulse locations were used for each test setup in order to insure that all modes were excited. A series of 5 hammer blows were averaged to come up with a frequency response function at each placement. A medium-hard hammer tip was chosen as it provided a flat excitation spectrum within the frequency range of interest (up to about 200 Hz). As the accelerometer locations were moved to cover the entire plate at locations 1 and 2, at least one sensor was left in position from the previous test in order to provide continuity of the mode shapes. Several frequencies were chosen from each test to look at mode shapes. It is common to use the imaginary part of the frequency response function to map out the possible mode shapes. Tables 1-3 summarize these values for the three locations and several frequencies of interest.

Table 1: Normalized Frequency Response Function (imaginary part). Location 1, Sta. 8+24, 25 ft-long plate, divided into 3 parts for the modal survey (both invert and wall plates). See figure 3 for key to locations in table.

Loc.	**f=0.31 Hz**	**f=27.19 Hz**	**f=64.69 Hz**	**Loc.**	**f=60 Hz**	**f=64.69 Hz**	**f=90 Hz**	**Loc.**	**f=0.31 Hz**	**f=6.88 Hz**	**f=64.69 Hz**
1	-0.49	-0.04	1.0	**11**	-0.06	-1.0	0.04	**111**	1.0	-1.0	0.39
2	-0.27	0.04	0.71	**22**	-0.12	-0.91	0.05	**222**	0.05	-0.79	0.13
3	0	0.71	0.48	**33**	0.32	-0.68	-1.0	**333**	0.05	-0.71	-0.58
4	-1.0	-1.0	0.38	**44**	-1.0	-0.15	0.39	**444**	0.41	-0.93	-0.48
5	-0.04	0.43	-0.33	**55**	0.09	0.0	-0.71	**555**	0.55	-0.79	-0.94
6	-0.18	-0.25	-0.81	**66**	0.51	0.59	-0.38	**666**	0.36	-0.57	-1.0
7	0.14	0.50	-0.62	**77**	0.03	0.82	0.01	**777**	0.23	-0.50	-0.61
	f=0.63 Hz	**f=4.38 Hz**	**f=64.69 Hz**		**f=0.31 Hz**	**f=59.69 Hz**	**f=64.69 Hz**		**f=0.31 Hz**	**f=59.69 Hz**	**f=64.69 Hz**
A	-0.13	1.0	0.65	**AA**	0.66	0.23	0.69	**AAA**	0.70	0.23	0.69
B	-0.50	-0.33	1.0	**BB**	1.0	-0.08	0.28	**BBB**	1.0	-0.08	0.28
C	0.38	0.44	0.96	**CC**	-0.26	-0.31	0.03	**CCC**	-0.26	-0.31	0.03
D	0.0	-0.22	0.96	**DD**	0.13	-0.38	-0.31	**DDD**	0.13	-0.38	-0.31
E	0.63	0.44	0.87	**EE**	-0.91	-0.08	-0.78	**EEE**	-0.91	-0.08	-0.78
F	-0.25	0.33	0.70	**FF**	0.43	-0.77	-0.75	**FFF**	0.43	-0.77	-0.75
G	1.0	-0.56	0.52	**GG**	-0.17	1.0	-1.0	**GGG**	-0.17	1.0	-1.0

Table 2: Normalized Frequency Response Function (imaginary part). Location 2, Sta. 8+94, 25 ft-long plate, divided into 3 parts for the modal survey (both invert and wall plates). See figure 3 for key to locations in table.

Loc.	f=0.31 Hz	f=45 Hz	f=64.69 Hz	Loc.	f=0.31 Hz	f=48.13 Hz	f=64.69 Hz	Loc.	f=0.31 Hz	f=48.12 Hz	f=64.69 Hz
1	1.0	-0.04	-0.06	**11**	-0.13	0.07	-0.92	**111**	0.94	0.0	-0.24
2	0.0	-0.02	0.15	**22**	0.63	-0.87	-1.0	**222**	0.33	-0.04	-0.21
3	-0.20	-1.0	0.82	**33**	0.75	-1.0	0.31	**333**	0.56	0.0	-0.63
4	0.0	0.28	0.70	**44**	0.33	0.73	0.65	**444**	0.11	0.56	-0.52
5	-0.40	-0.17	0.85	**55**	-1.0	-0.40	0.62	**555**	1.0	1.0	-0.02
6	-0.20	0.15	0.97	**66**	0.25	-1.0	0.04	**666**	-0.22	-0.70	-0.06
7	-0.20	-0.16	1.0	**77**	0.50	-0.33	-0.96	**777**	0.22	0.56	1.0
	f=0.31 Hz	**f=1.88 Hz**	**f=64.69 Hz**		**f=0.31 Hz**	**f=20.0 Hz**	**f=64.69 Hz**		**f=0.31 Hz**	**f=20.0 Hz**	**f=64.69 Hz**
A	1.0	-0.22	1.0	**AA**	-0.40	-0.88	0.80	**AAA**	-0.53	-0.57	-0.49
B	0.33	0.22	0.76	**BB**	-0.10	-0.88	0.63	**BBB**	-0.27	-1.0	-0.29
C	-0.17	0.44	0.48	**CC**	-1.0	-0.88	0.31	**CCC**	-0.67	-0.50	-0.08
D	0.33	0.33	0.27	**DD**	0.30	-1.0	.014	**DDD**	-1.0	-0.64	0.14
E	-0.67	0.33	-0.09	**EE**	0.60	-0.75	-0.23	**EEE**	0.33	-0.71	0.25
F	0.50	-0.33	-0.36	**FF**	-0.80	-0.33	-0.49	**FFF**	0.33	-0.50	0.41
G	0.17	-1.0	-0.55	**GG**	0.30	-0.75	-1.0	**GGG**	0.47	-0.43	1.0

Table 3: Normalized Frequency Response Function (imaginary part). Location 3, Sta. 9+66, One single 8 ft-4 in floor and wall plate. See figure 3 for key to locations in table.

Loc	f=0.31 Hz	f=20 Hz	f=64.69 Hz
1	0.18	1.0	-0.58
2	-0.36	0.29	-0.25
3	-1.0	0.71	0.13
4	0.82	0.86	0.46
5	-0.61	-0.29	0.75
6	-0.82	0.29	0.75
7	-0.79	0.57	1.0
	f=1.25 Hz	**f=59.69 Hz**	**f=64.69 Hz**
A	0.63	1.0	0.97
B	-0.38	0.64	1.0
C	-0.63	0.64	0.89
D	0.50	0.57	1.0
E	0.50	0.07	0.82
F	1.0	0.50	0.89
G	0.13	1.0	0.95

Operational Testing

Based on results of the modal testing and construction details of the spillway, four uniaxial strain gages and four low-profile accelerometers were installed on the spillway invert for testing with flow conditions. The strain gages were manufactured by Vishay MicroMeasurements and were 3-wire, 350-ohm uniaxial gages with a 0.125-in active length. They are manufactured mounted on a steel shim and waterproofed, ready to be installed. The gages were then spot welded to the spillway invert plate at location 1. Locations adjacent to plug welds were chosen as these were in probable high stress zones with stress concentration factors of up to 3. Two gages were mounted near the spillway centerline, figure 5, and two gages were mounted at the midspan of the left side plate at location 1, figure 6. Additional lengths of lead wires were spliced on to allow the signals to be monitored at a central location topside. Four low-profile accelerometers were also installed on the spillway invert. Two sensors were mounted near the location of the strain gages in areas where large deflections were likely due to loss of foundation material beneath the plate. The other two sensors were mounted in similar locations, but downstream near the runout section at station 9+66. The accelerometers were mounted directly to the $^{5}/_{16}$-in steel plates by drilling and tapping for a 10/32 mounting stud, figure 7. The accelerometers had 40 ft of integral cable so no splicing was necessary to get the leadwires up and out of the spillway channel. Once all the sensors had been located and installed, the sensors and leadwires were covered with a marine epoxy, typically used in fiberglass repair on boat hulls. This epoxy bonds well with the steel plates and provides ample waterproofing for the sensors and mechanical protection from the flowing water, figure 8. Four portable accelerometers on magnetic bases were located on the side walls adjacent to the plate locations where the invert instrumentation was installed, figure 9. These accelerometers were located above the water line and were installed to indicate whether the side wall plates would be excited by the relatively shallow flows within the spillway. This coating was allowed to cure for over 12 hours at well over the minimum temperatures required. The following day, the sandbags and other leakage control measures were removed from the spillway channel, the sensors were wired into the computerized data acquisition system and additional preparations for the flow tests were completed. Figure 10 shows the lower end of the spillway with 1500 ft^3/s discharging into the Rio Chama.

Data was collected using a laptop computer and an IOTech Wavebook 516, portable data acquisition system, figure 11. Power was provided by a portable generator. Excitation power was applied to the accelerometers and the strain gages. The strain gages were calibrated using shunt resistor techniques, and then the offsets were zeroed out in preparation for the spillway releases. Leakage was estimated at 25-50 ft^3/s, so a shallow flow was present over the spillway invert during calibration and zeroing. The spillway gate was then opened to approximately 3 ft, and with the reservoir elevation at 6899.8 ft, this corresponded to about 2700 ft^3/s according to available discharges curves. This flow was maintained for about 10 minutes. The startup was recorded, and then an additional 5 minutes of data were recorded once the flow had stabilized. Additional documentation by photo and video was performed by others. The spillway gate was then closed. A physical inspection of the sensor locations and wiring revealed that the two accelerometers at plate location 3 had experienced a failure in the epoxy coating over the lead wires coming up the side wall and had been damaged most likely to fatigue of the wire. All other sensors appeared to be in good condition. The data files were reviewed to insure that data had been recorded before proceeding to the second test flow.

The gate was then opened to about 18-in, allowing about 1500 ft^3/s to be released. The startup was recorded, along with about 5 minutes of data once the flow conditions had stabilized. The gate was closed. The instrumentation was again visibly inspected and no additional failures appeared to have occurred. Data files on the computer were checked to insure that data had been collected and saved. Once these precautions had been taken, the test was deemed to be complete and the sensors were disconnected from the data acquisition system and the equipment was packed up.

Results from the flow tests are presented as samples of the acceleration and strain time series with corresponding frequency spectra, figures 12-19. Additional analysis of the data will be presented in the section to follow.

Analysis and Discussion

Flow tests were preformed on the spillway at El Vado Dam. The structure is constructed of welded-steel plates on a structural steel frame that sits on an earth foundation and which is approaching 75 years in-service. Major rehabilitation was performed in the past (over 50 years ago) and the standard maintenance approach has been to attempt to repair cracks and broken welds with weld repairs. These repairs have been somewhat successful, however many repairs have resulted in additional cracks to the heat-affected zones. Various techniques of welding and bolting plates to try and repair cracks or gaps in the lining have had some success. However, plates have been overstressed with some of these repairs and failures to the lining remain, figure 20.

The operational history on this spillway has apparently been quite infrequent. Historical records indicate maximum flows on the order of 5000-6000 ft^3/s, with rare operational events of any amount. The flows chosen for these tests (up to 2500 ft^3/s) were chosen to remain within current operating restrictions. These current tests were designed in order to observe the interaction of the spillway lining plates with flow and to determine if flow-induced fatigue failures of the plates are a possibility. One very large unknown that remains after the test, is that the spillway is made up of hundreds of plates and so it does not necessarily act as a single structural unit. To this extent, choosing plates to instrument is difficult as not all plates were accessible and the true underlying condition of the plates, their welds, the substructure, and foundation is not fully known.

The critical welded joints – at least from the standpoint of existing failures, appear to be the many plug welds throughout the structure. The result of the analyses reported herein suggest that thermal stresses on the plates and plug welds likely play a significant role in creating stress cycles capable of causing fatigue-related failures.

Thermal Stresses

The location of the spillway is such that it is exposed to heating from solar radiation, which induces thermal stresses. Temperatures of the metal likely exceed 100 degrees Fahrenheit during the summer months. A temperature differential of 50 degrees Fahrenheit was assumed for a typical diurnal cycle. The resulting thermal stress induced for a single spillway lining plate was found to be 12,622 lb/in^2. The spillway invert lining plates are 25 ft long in the streamwise direction, and 8-ft 4-in wide laterally, see drawing A-197 (fig. 2). The support afforded by the underlying steel support structure, results in the plates being unsupported over 8 ft 4 in square areas (assuming large voids exist under specific plates). Assuming the boundaries of these squares are fixed (by virtue of butt and plug welds), large deflections of the plates will occur. From observations at the dam, half cycle vertical deflections, 8 ft 4 in long occurred in the invert plates between the fixities due to thermal effects. Buckling, an elastic instability occurs in flat plates when they are subjected to compressive loading in the plane of the plate. When a critical value of compressive stress occurs, the plate deflects but is able to support this critical stress. If the load is removed the plate deflects back to its initial shape, no permanent deformation occurs. However, failure, complete collapse, or permanent deformation may occur if the deflected shape is excessive. The theoretical thermal buckling stress is 1,405 lb/in^2 and with plug welds on 12-in-centers the resulting bending moment at a plug weld is 5,268 in-lb. As a result of this bending moment, the stress in the plug welds in the vertical direction is 32,426 lb/in^2. However, the ultimate shear stress of the plug weld is only 34,200 lb/in^2; therefore thermal stresses are expected to cause failure of the plug welds. From inspection of the plug welds in the spillway lining plates, cracks around the circumference of the plug welds have been seen. In fact several of the plug welds along the lower reaches of the spillway have failed entirely. The bending stress in the longitudinal butt welds in the plates was found to be 26,972 lb/in^2, which is below the 60,000 lb/in^2 ultimate stress of the weld in tension and no cracks have been found in the longitudinal butt welds in the invert lining plates suggesting failure of butt welds due to thermal stresses is not likely.

Dead and Hydrostatic Loading

The dead weight of the 5/16-in-thick lining plates result in a bending stress of 2,773 lb/in^2, when this is combined with the thermal stress the total stress is 4,178 lb/in^2, not enough to cause failure. However, if large voids exist beneath the lining plates, hydrostatic loading will result in high stresses, assuming the foundation material provides no reaction support. Considering a linear response of the plate to the loading, a hydrostatic head (or flow depth) of 4 ft-3 in combined with the dead load produces stresses of 60,640 lb/in^2, which would result in plate failure. Failure will occur over the middle sections of the edges of the plate and cracking will rapidly propagate out to the corners. However, a non-linear analysis, which considers membrane (tension) stresses in the plate combined with bending stresses resulted in a hydrostatic head of approximately 13 ft-6 in to cause failure of the plate. In this case the non-linear analysis is more appropriate than the linear analysis as the plate deflections are considered to be large (greater than the plate thickness).

Based on the non-linear analysis, a net hydrostatic head or hydrostatic differential of 13 ft-6 in is expected to cause lining plate failure. This could result from either flow depths in the spillway exceeding 13 feet along the upper reach of the spillway or from uplift due to hydrostatic pressures beneath the lining plates along the lower reach of the spillway. The difference in elevation between the upstream and downstream ends of the spillway is 98 ft. Therefore, if openings in the foundation material below the invert of the spillway result in a minimum uplift hydrostatic head of 27 ft at any plate with a spillway water depth of 13 ft-6 in, those plates are expected to fail.

Side plates

Hydrostatic head, underneath or behind the lining plates, due to leakage in upper sections of the spillway, results in loading on the side plates and creates the potential for failure. Along the location where instrumentation was located, one of the side panels with existing cracks (presumably due to corrosion) deflected outwards and backing material was washed out during testing at 2700 ft^3/s, figure 21. Normal drain flows at least doubled in volume and went from a relatively clear to cloudy appearance during testing. Another side panel further upstream was observed to bulge with deflections approaching 1 ft resulting in permanent deformation after the flow test. The theoretical stresses for this load condition indicate potential failure of the plate consistent with observations during operational testing.

Dynamic Stresses During Testing

The dynamic stresses recorded for the test flows were very low. Stress time histories along with stress range pair histograms were developed using the rainflow counting method (ASTM E 1049-85). This method of data analysis is useful to evaluate fatigue as it reduces a spectrum of varying stress into a set of simple stress reversals, allowing application of Miner's rule to determine fatigue life of a structure with complex loading. Strain gage 2 was not working properly and will be disregarded in this analysis. Table 4 shows the mean stresses for the two different flow conditions. Figures 22-24 show stress range count histograms for the three working strain gages at each of the flow conditions tested. The stress range pairs follow fairly closely to a Gaussian distribution for this facility and the locations and flows tested. The maximum stress range recorded was 225 lb/in^2 for gage number 4. The stress range allowable for plug welds is 8,000 lb/in^2 for 2×10^6 cycles (i.e. infinite fatigue life); therefore fatigue failure for a discharge of 2,700 ft^3/s is not expected. In the case of maximum spillway discharges, the plates would likely be deflecting differently and it is not possible to extrapolate the measured stresses to higher discharges.

Table 4: Mean stresses in lb/in^2 for the two flow conditions tested.

Discharge (ft^3/s)	Mean Stress (lb/in^2)		
	Gage 1	Gage 3	Gage 4
1500	1533	792	1115
2700	1747	1209	1296

Vibration

Accelerations recorded during flow operations, while not definitive; do lead to some insight on how the structure reacts to excitation by flow. The data indicate that similar frequencies are excited by the flow as were seen during the modal survey impulse/response testing (in air). The sidewall construction is substantially stiffer than the invert plates and is reflected somewhat in the reduction of excitation seen during the flow events. At location 1, the upstream to downstream accelerometers on the sidewalls yielded an increase in acceleration at the most downstream location which is representative of the noticeable lack of backfill/foundation behind that plate. It appears that the downstream one-third of this plate may be freely hanging, suspended by the underlying structure but devoid of backfilled material.

Comments on Structural Integrity of the Spillway

Original design calculations for the spillway were not available and there was little information provided regarding operational history, although it appears the spillway has rarely been operated in the last 50 years. Based on the structural analyses it is likely that the original calculations assumed that the steel plates would remain supported on foundation material between the underlying steel support structures. This assumption would result in the hydrostatic loading being reacted uniformly by the foundation, with minimal stresses in the plates.

Over time, the foundation material has apparently compressed, migrated, and/or been removed entirely resulting in large voids under the invert lining plates and behind the wall plates. In fact voids have been identified during recent inspections. The voids (or at least unsupported plates) are also apparent when walking on the spillway as large deflections were observed for many of the plates. The modal analysis also gave indications of voids behind the plates due to large structural response from very small energy inputs. The loss of foundation reaction significantly changes structural performance. With voids under a large area of a single plate, the plate is supported only by the underlying framework. The resulting membrane and bending stresses in the plates will likely result in failure with around 13 ft-6 in of hydrostatic differential. To date, it appears there have been no large (near design flow) discharges through the spillway, and consequently failure has not occurred. However, if in the future a discharge producing flow depths greater than 13 ft-6 in, or an upward hydrostatic head differential approaching13 ft-6 in were to occur, the invert lining plates are expected to crack open allowing water to flow under the plates, causing further erosion of the foundation material and potential undercutting of the spillway.

Thermal stresses were apparently overlooked in the original design. These stresses are the most likely cause of observed or existing cracks around the plug welds since historical operations appears to be rather minimal. Failed plug welds could lead to a situation where much lower uplift hydrostatic differentials would cause failure (e.g., if all the plug welds for a single plate failed, the effective unsupported area in an uplift condition would significantly increase).

The modal analyses and dynamic testing results suggest that there are indeed large voids under a number of the invert lining plates. However, the dynamic stresses resulting from the discharge tests were found to be minimal and would not likely produce fatigue failure. The strain gages that were monitored during these operational tests were at locations where there appeared to be adequate foundation materials to support the plate (i.e. there was not evidence of a noticeable void in the area of the strain gages). Nevertheless, with higher discharges the fluctuating stresses could be sufficiently large to result in propagation of existing cracks which would further increase failure potential due to hydrostatic loading.

The findings from this report indicate that it is not reasonable to rely on the spillway, in the existing condition, for discharges producing flow depths greater than 13 ft at any location along the spillway. Furthermore, recognizing the potential for large uplift pressures previously mentioned, even flow depths less than 13 ft may not be acceptable. In any case, it is clear that if foundation material cannot be maintained under and behind the spillway lining plates to provide the required additional support, then structural integrity of the spillway will be insufficient. This issue, in combination with existing plug weld failures due to thermal stresses, suggests significant design flaws.

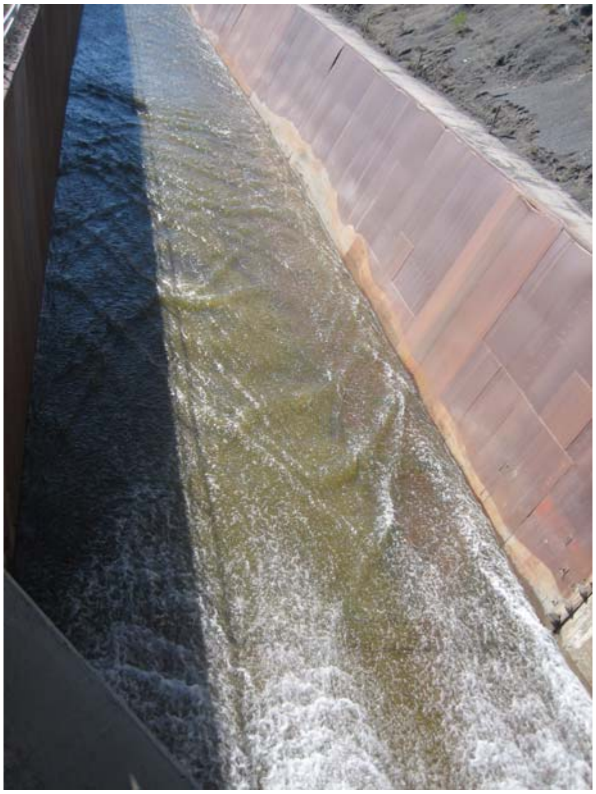

a) leakage through gate in early June 2008

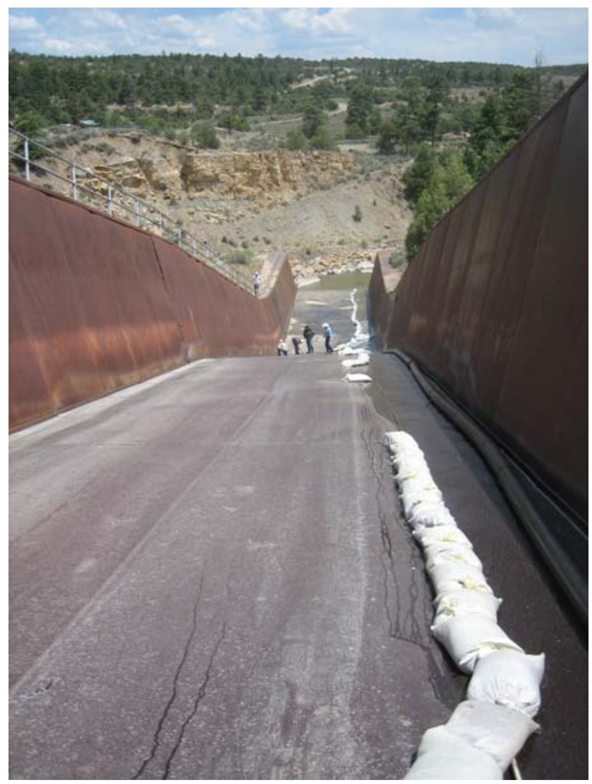

b) leakage controlled and diverted to the right side of the spillway invert.

Figure 1: Views down the steel-plate-lined spillway at El Vado Dam.

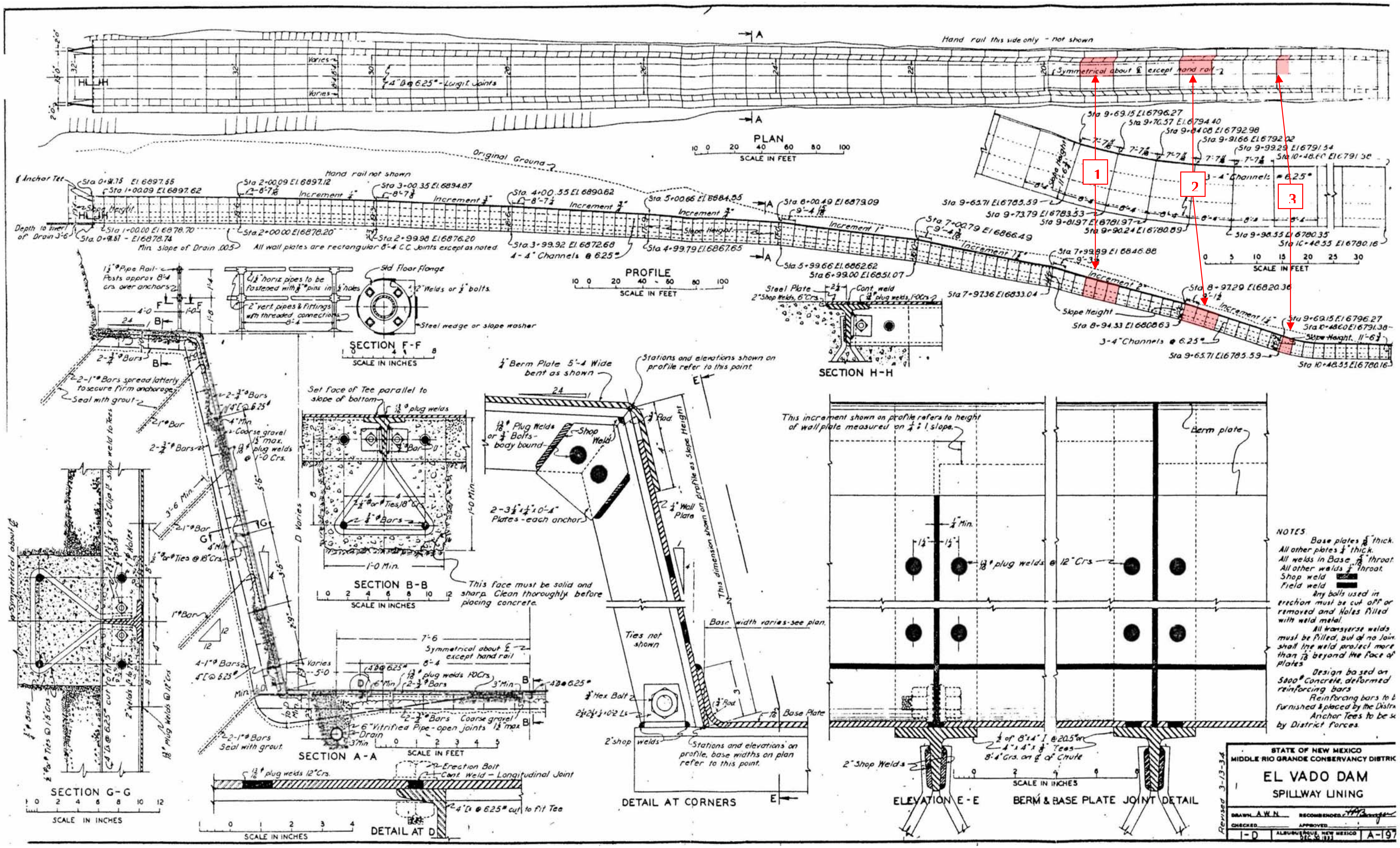

Figure 2: General construction detail. Note spillway profile with the three locations (noted in shaded red) where the modal testing and sensors were installed.

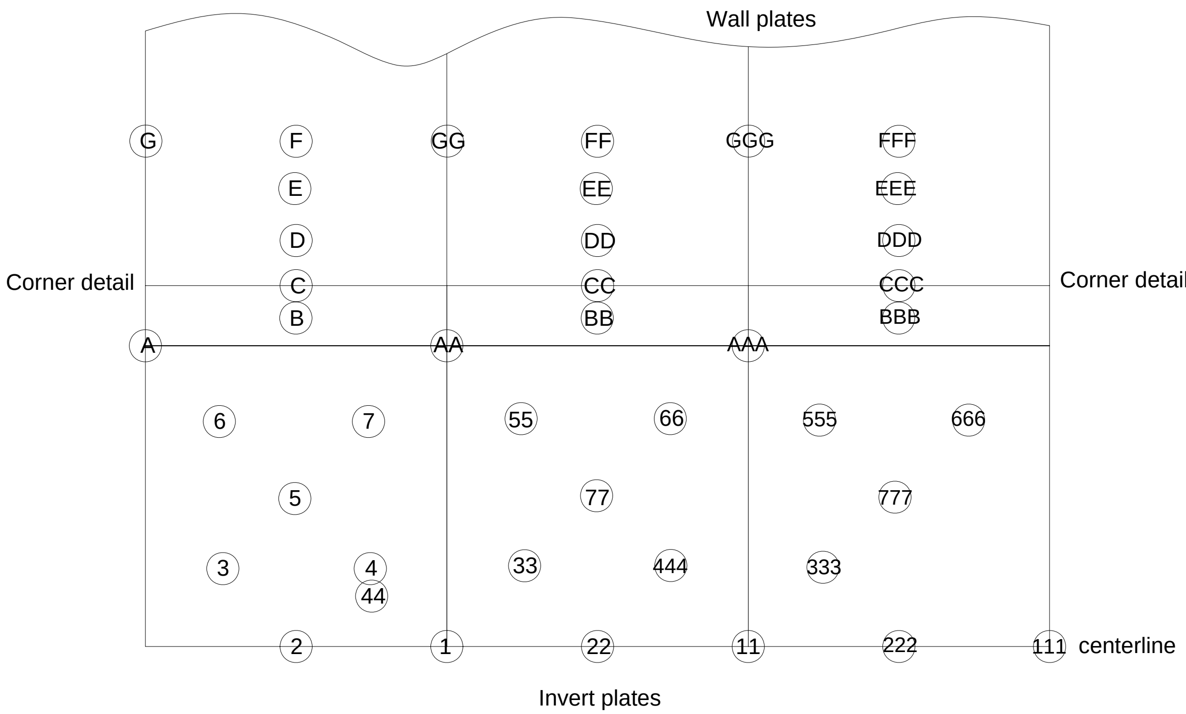

Figure 3: Developed view of accelerometer positions for the modal survey, location 1 and 2. Location 3 is a single 100-in by 100-in plate represented by one third of the figure above.

Figure 4: Placement of accelerometers on invert plates for impulse/response modal testing.

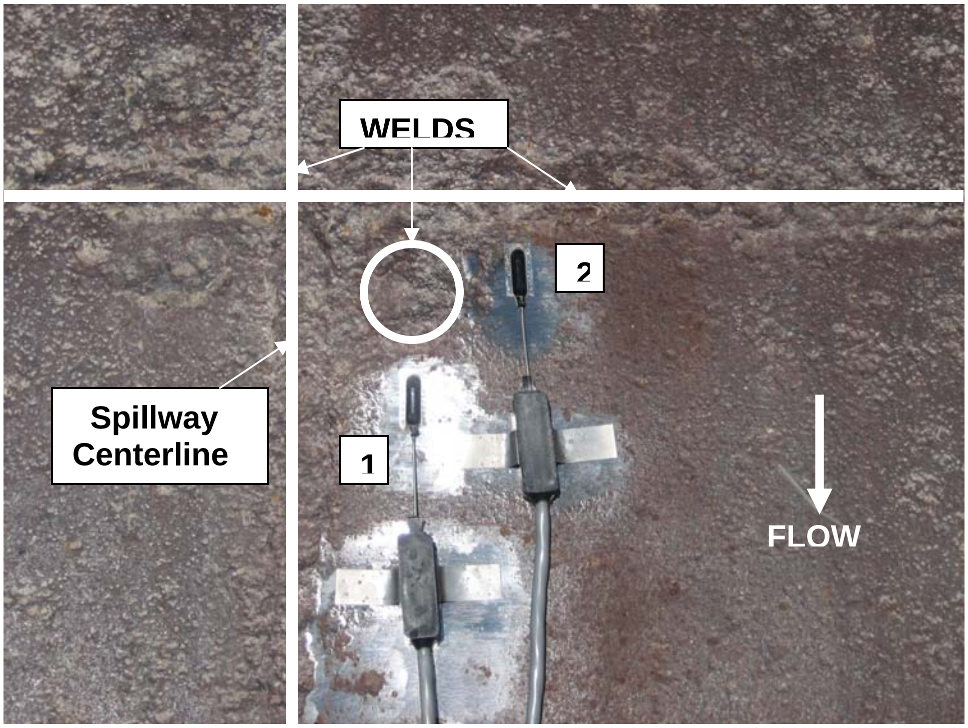

Figure 5: Strain gages 1 and 2 at Location 1, near spillway centerline.

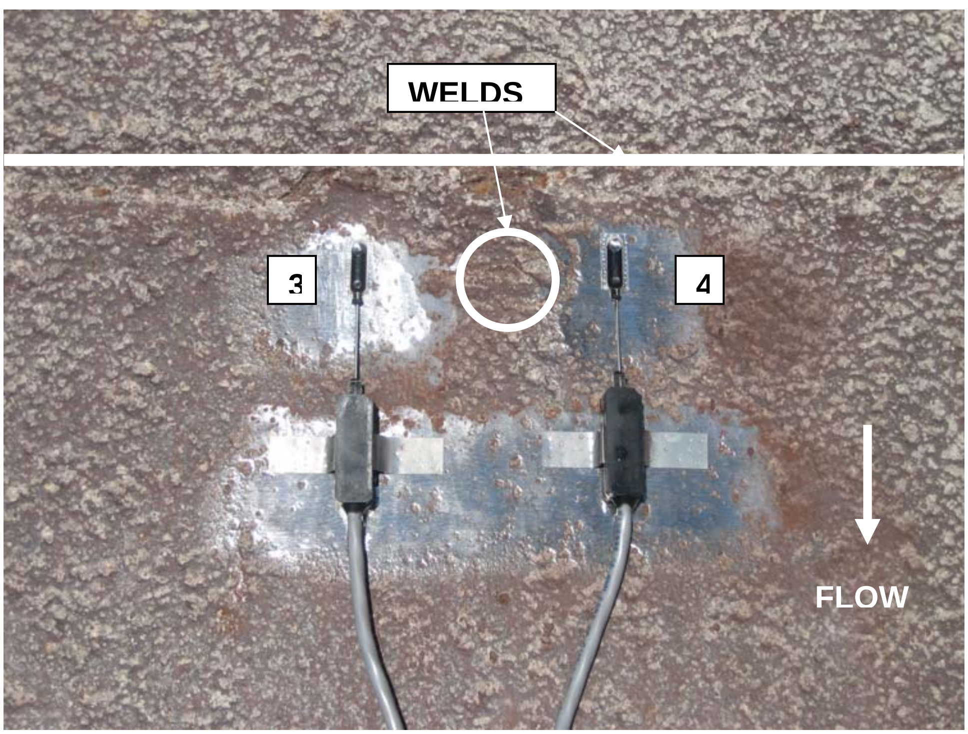

Figure 6: Strain gages 3 and 4 at Location 1 near midspan of left invert plate.

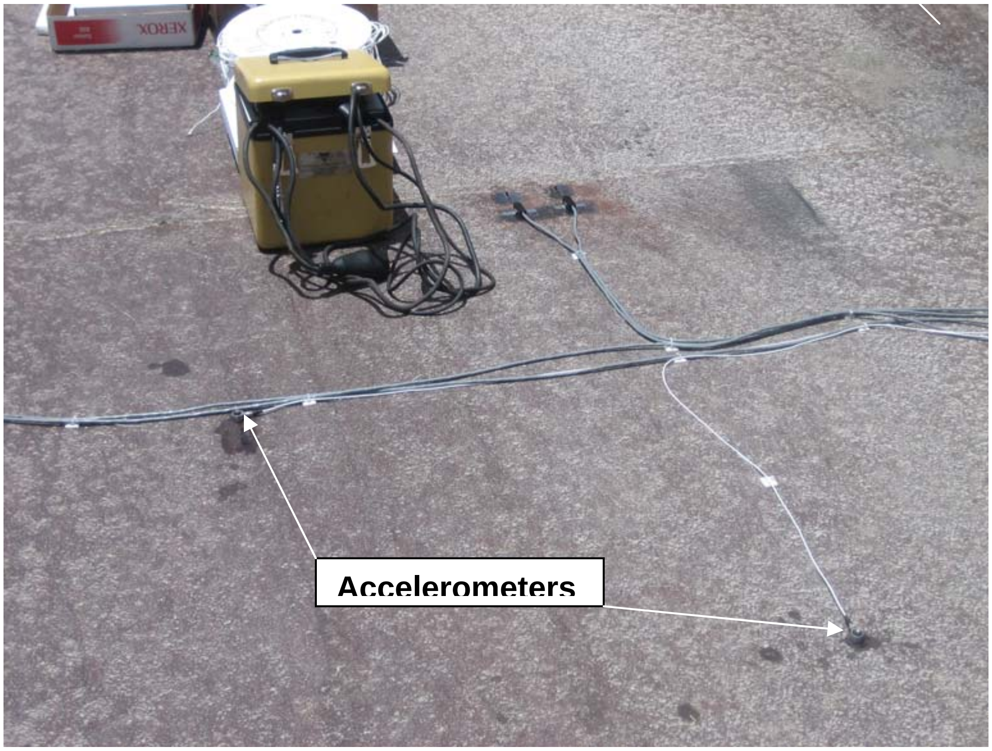

Figure 7: Accelerometers were attached directly to invert plate using a threaded stud.

Figure 8: Marine epoxy coating applied over strain gages, accelerometers, and lead wires.

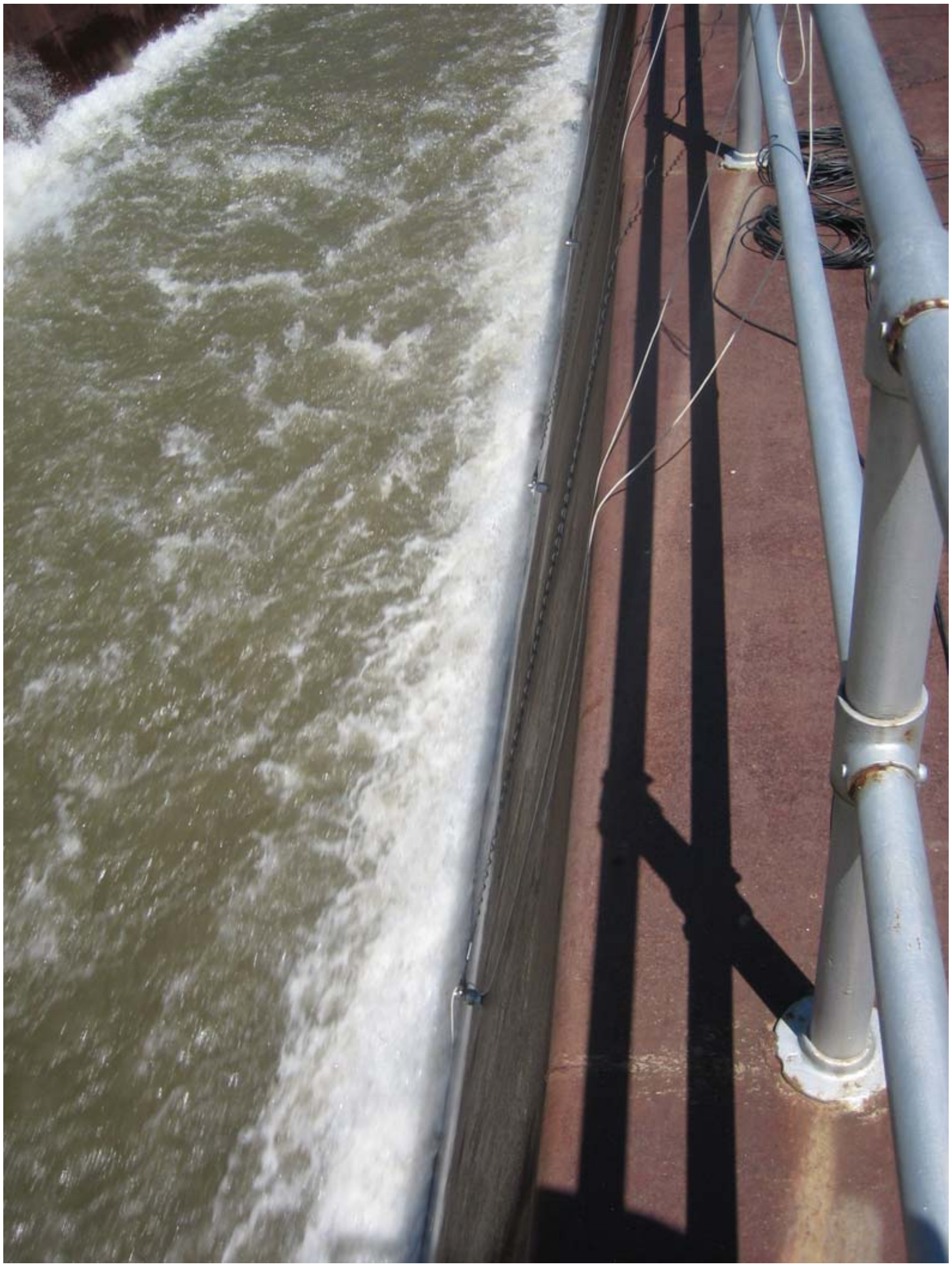

Figure 9: Flow of 2700 ft^3/s passing by location 1, note sidewall accelerometers above water level.

Figure 10: Spillway operating at 1500 ft^3/s. Chute flow drops into Rio Chama below.

Figure 11: Data acquisition system setup along side of spillway.

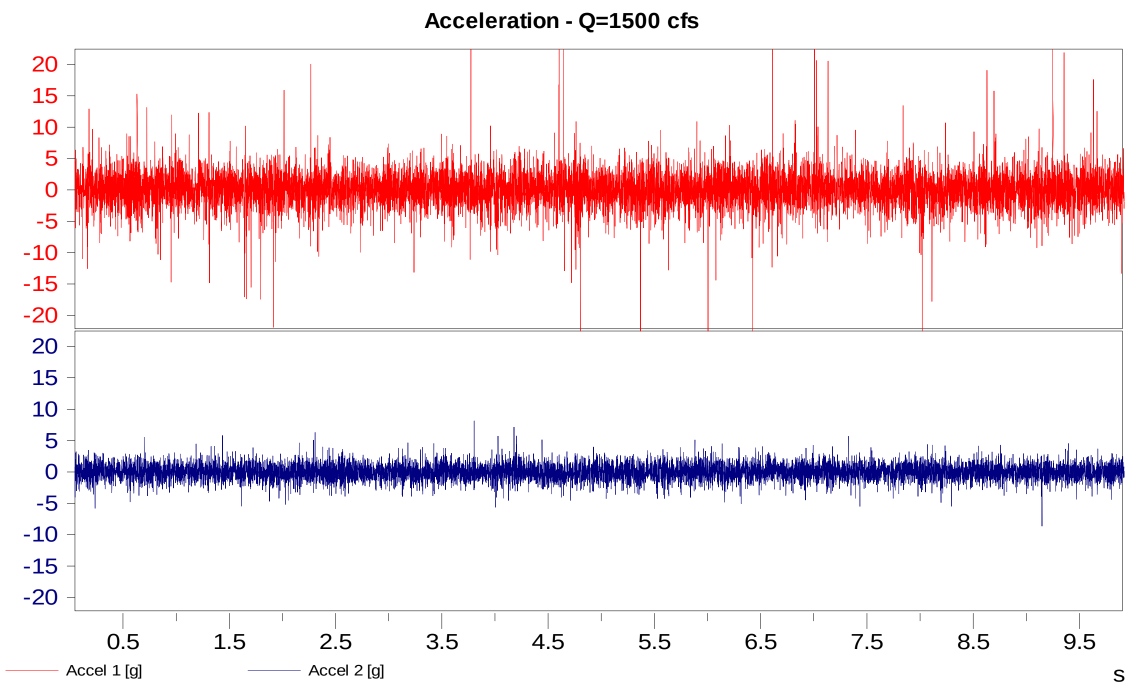

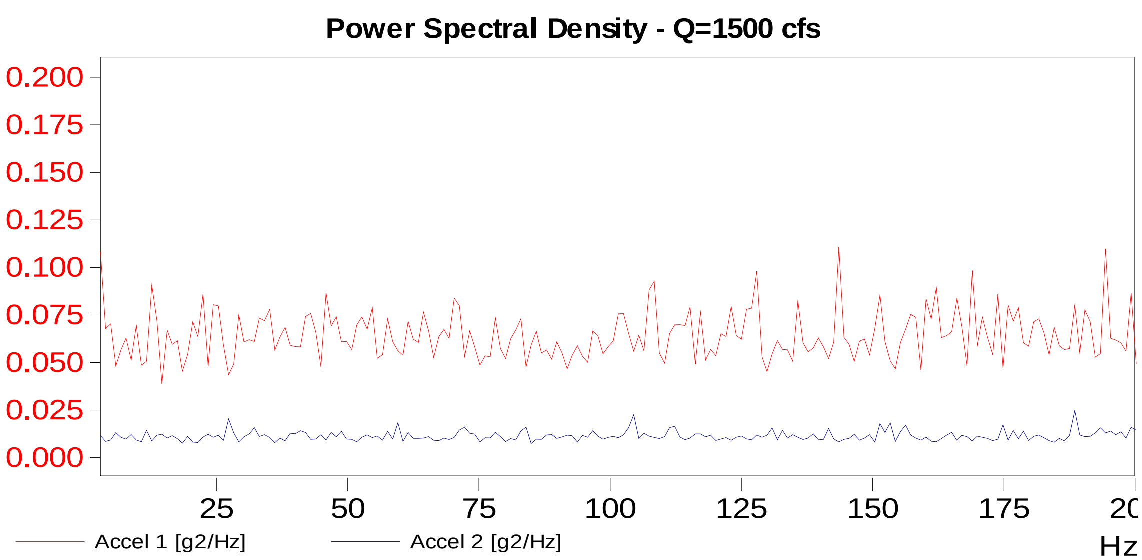

Figure 12: Invert accelerometers at location 1, Q=1500 ft^3/s, sample time series and peak Power Spectral Density. Major frequency peaks: Accel 1(12.7, 22.46, 45.9, 108.4, 127.93, 143.55, 194.34), Accel 2 (27.34, 59.57, 104.49, 188.48).

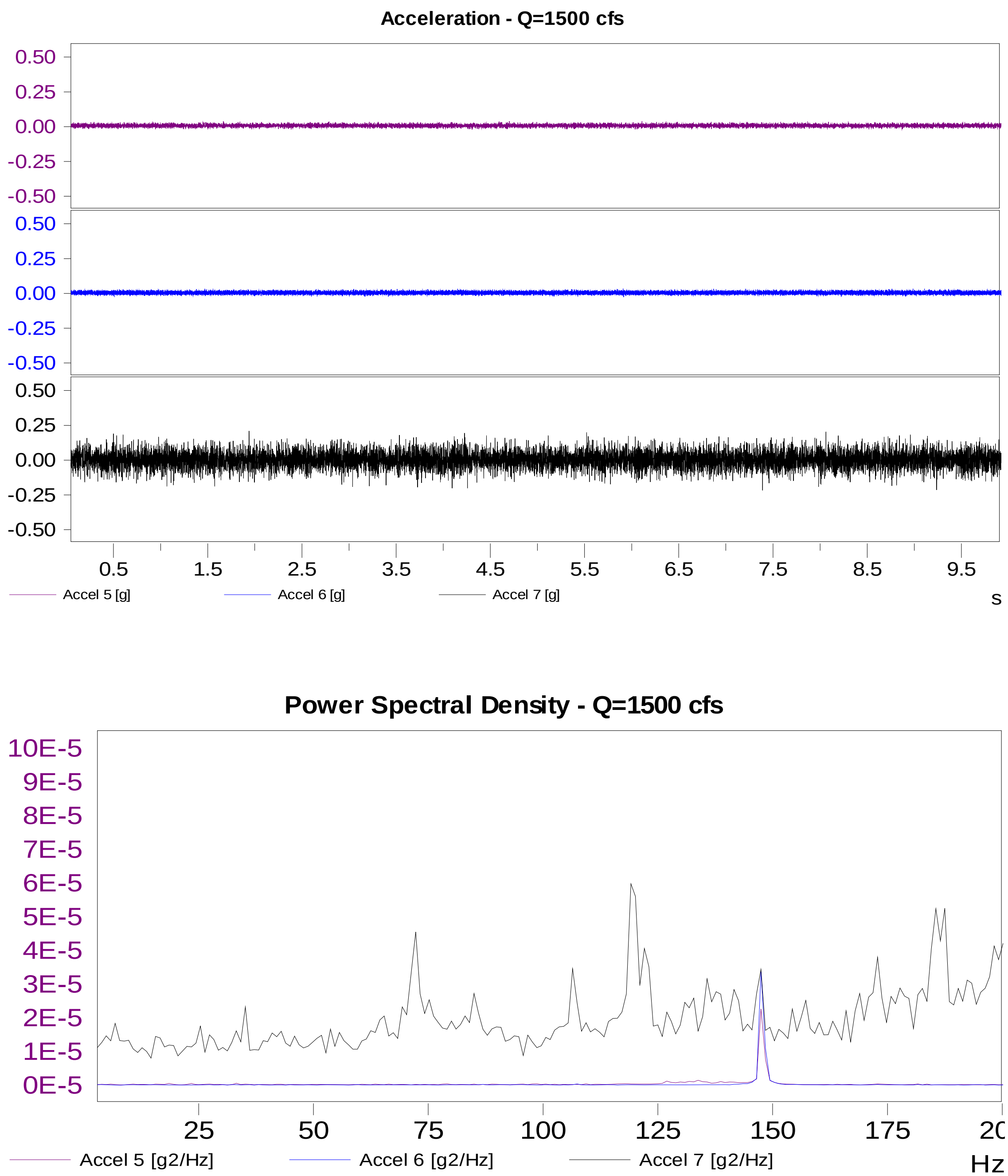

Figure 13: Wall mounted accelerometers at location 1, Q=1500 ft^3/s, sample time series and Power Spectral Density. Major frequency peaks: Accel 5 (147.46), Accel 6 (147.46), Accel 7 (6.84, 35.14, 72, 27, 106.45, 119.14, 147.46, 172.85, 185.55).

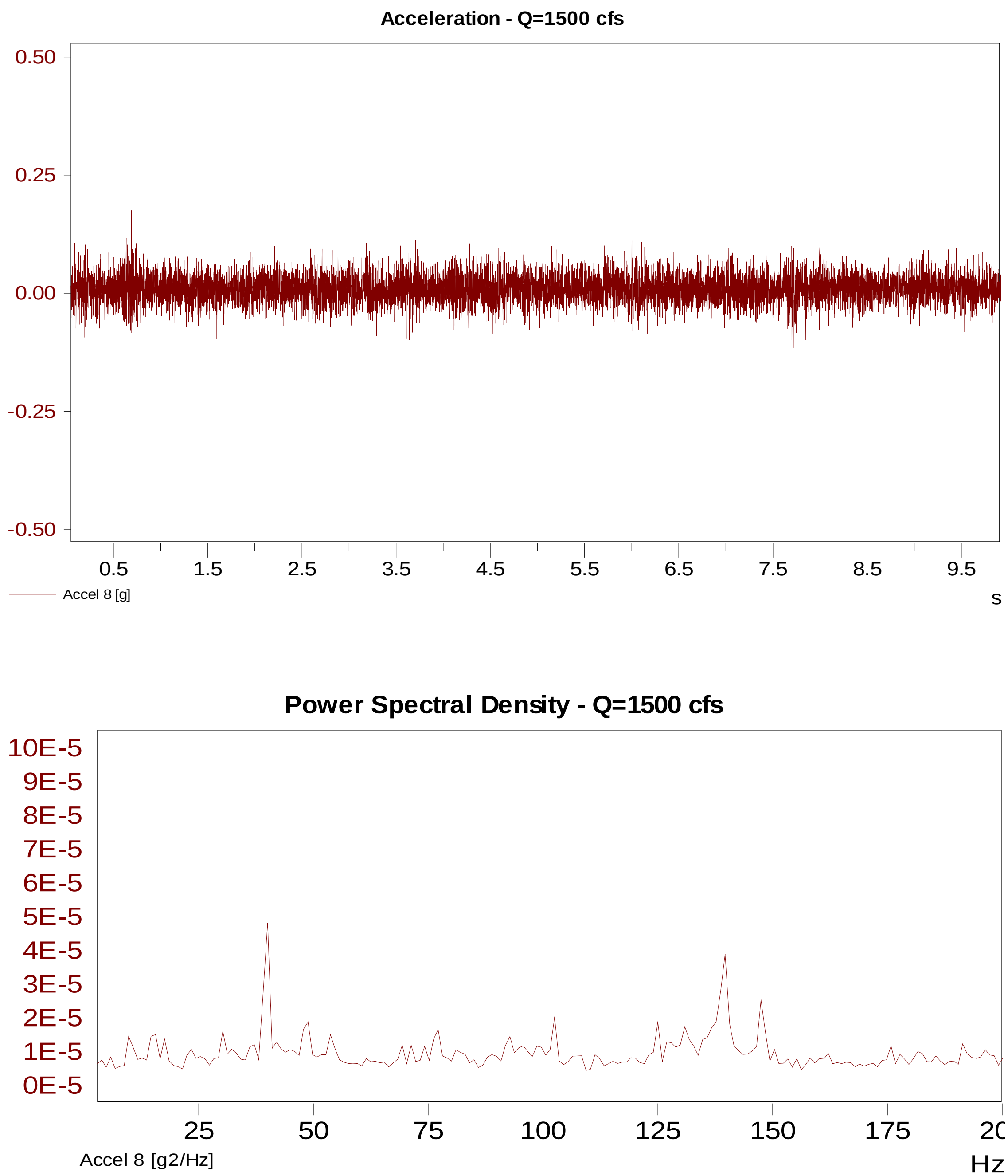

Figure 14: Wall-mounted accelerometer at location 3, Q=1500 ft^3/s, sample time series and Power Spectral Density. Major frequency peaks: Accel 8 (40.04, 139.65, 147.46).

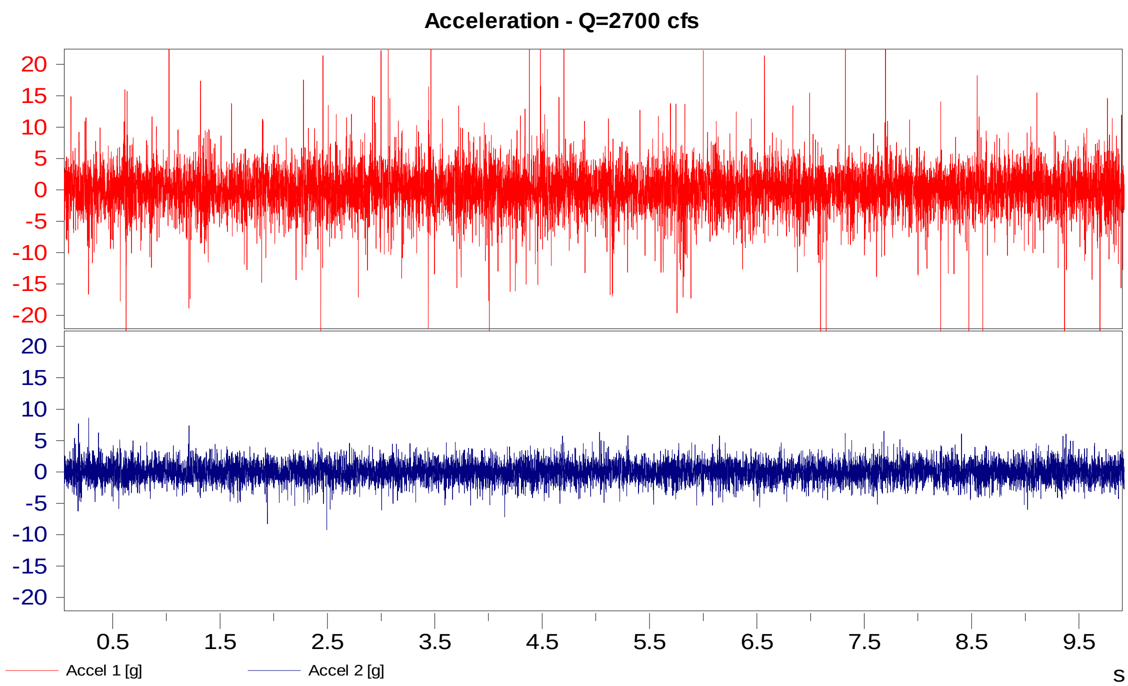

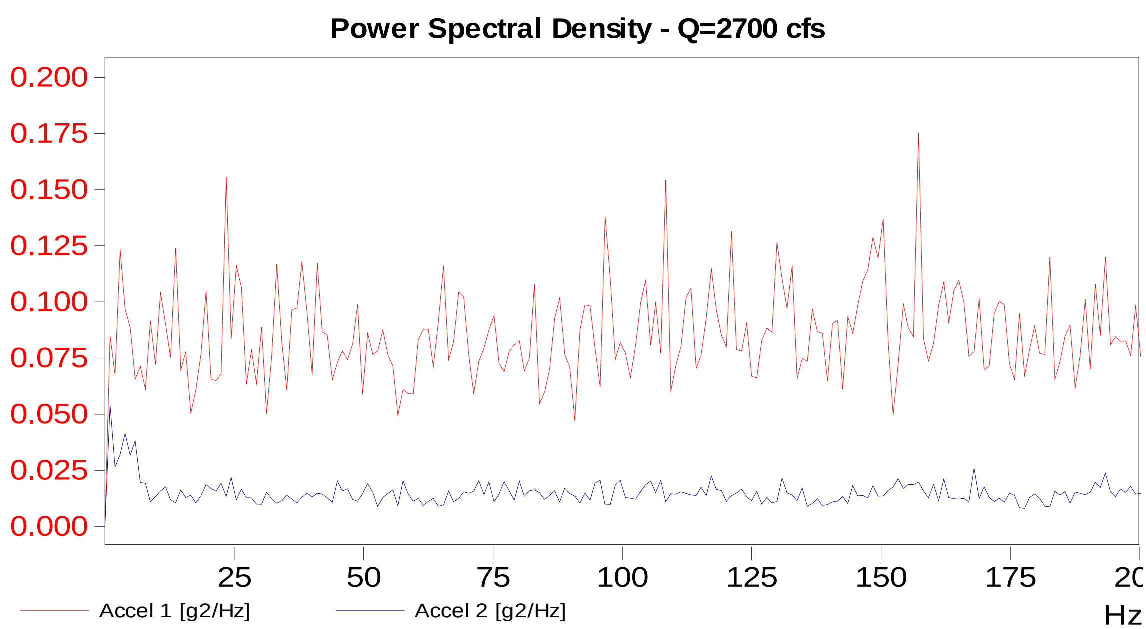

Figure 15: Invert accelerometers at location 1, Q=2700 ft^3/s, sample time series and peak Power Spectral Density. Major frequency peaks: Accel 1 (2.93, 13.67, 23.44, 33.20, 65.44, 96.68, 108.4, 121.09, 150.30, 157.23), Accel 2 (0.98, 3.91).

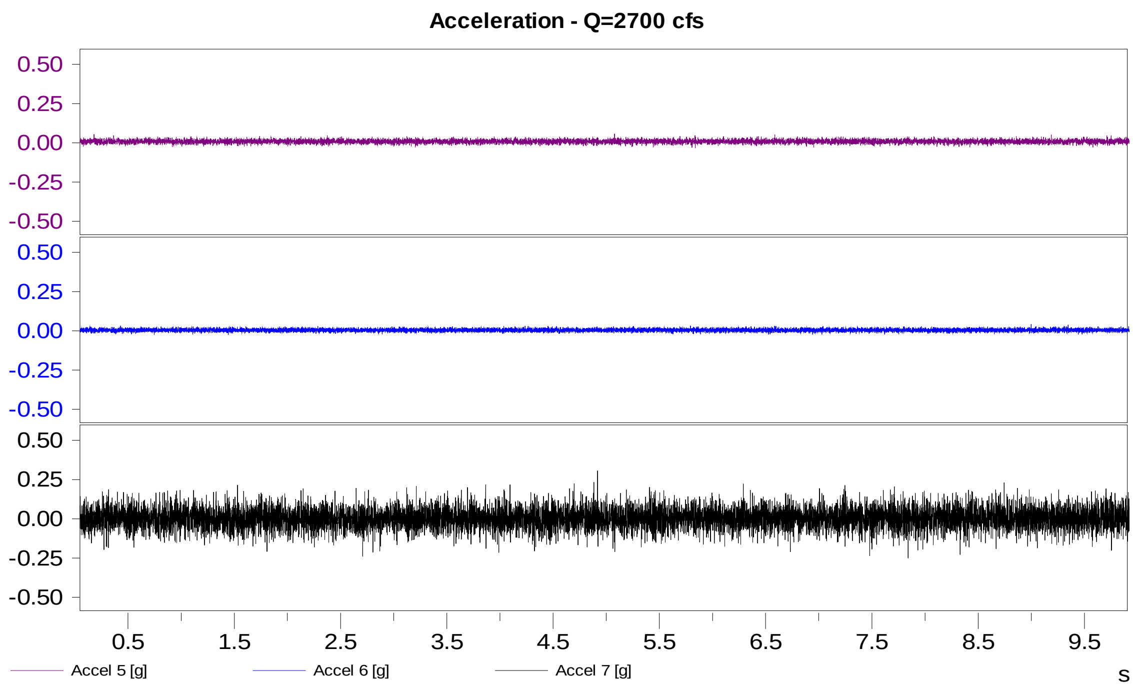

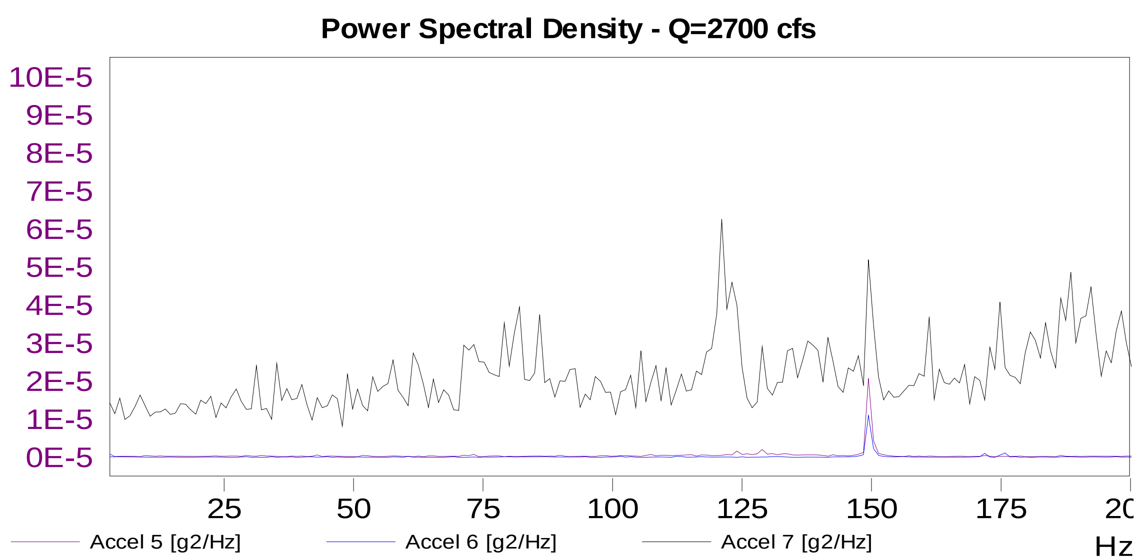

Figure 16: Wall mounted accelerometers at location 1, Q=2700 ft^3/s, sample time series and Power Spectral Density. Major frequency peaks: Accel 5 (149.41), Accel 6 (149.41), Accel 7 (121.09, 149.41).

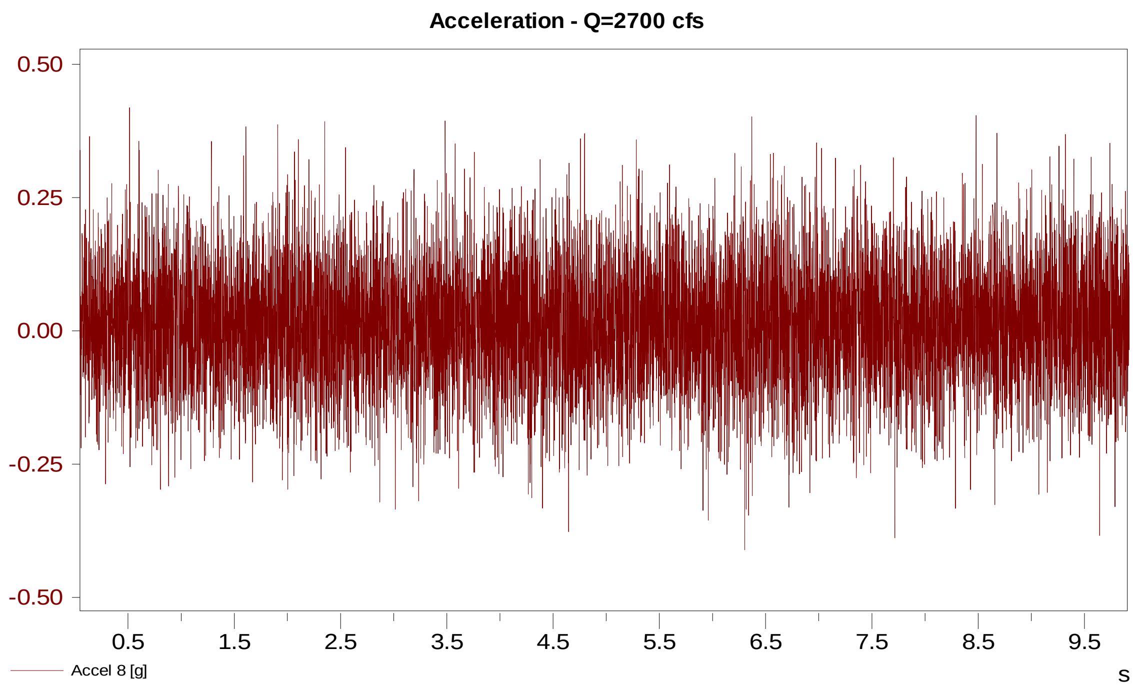

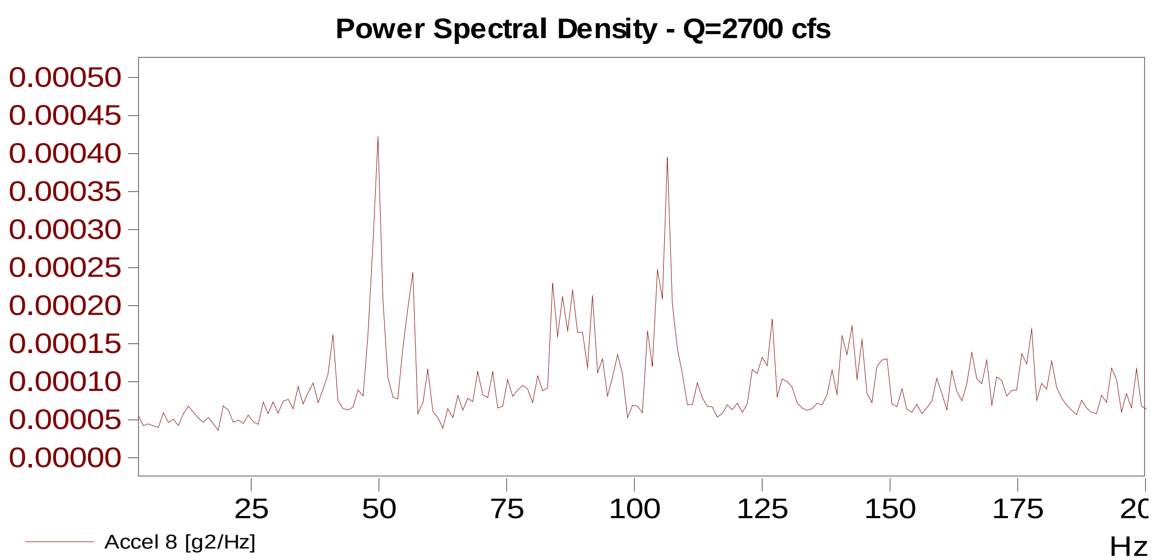

Figure 17 Wall-mounted accelerometer at location 3, Q=2700 ft^3/s, sample time series and Power Spectral Density. Major frequency peaks: Accel 8 (41.02, 49.80, 56.64, 106.45).

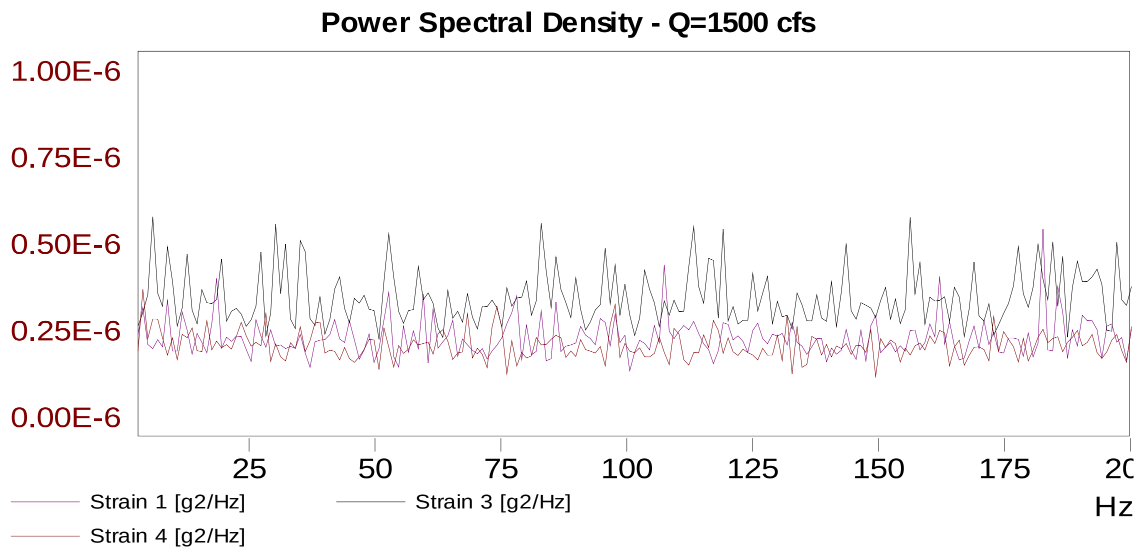

Figure 18: Power Spectral Density of strain gage time series showing major frequencies for Q=1500 ft^3/s. Major frequency peaks: Strain 1 (3.91, 8.79, 18.55, 52.73, 78.13, 107.42, 162.11, 182.62), Strain 3 (5.86, 30.27, 35.16, 52.73, 83.01, 113.28, 119.14, 143.55, 156.25), Strain 4 (3.91, 28.32, 74.22, 97.55, 131.84, 172.85).

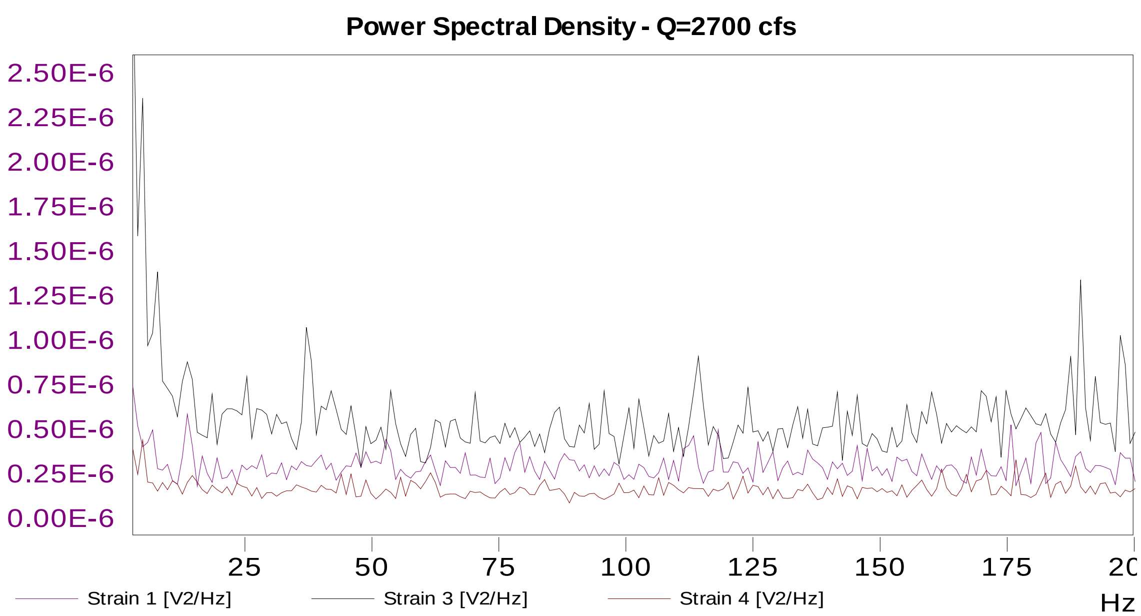

Figure 19: Power Spectral Density of strain gage time series showing major frequencies for Q=2700 ft^3/s. Major frequency peaks: Strain 1 (6.84, 13.67, 118.16, 175.76), Strain 3 (4.88, 7.81, 37.11, 114.26, 189.45, 197.27), Strain 4 (4.88, 14.65, 61.62, 176.76).

Figure 20: Attempts to close cracks and broken welds by covering with plates.

Figure 21: Head differential behind wall lining plates producing flow of water and material out into the spillway channel at 2700 ft^3/s.

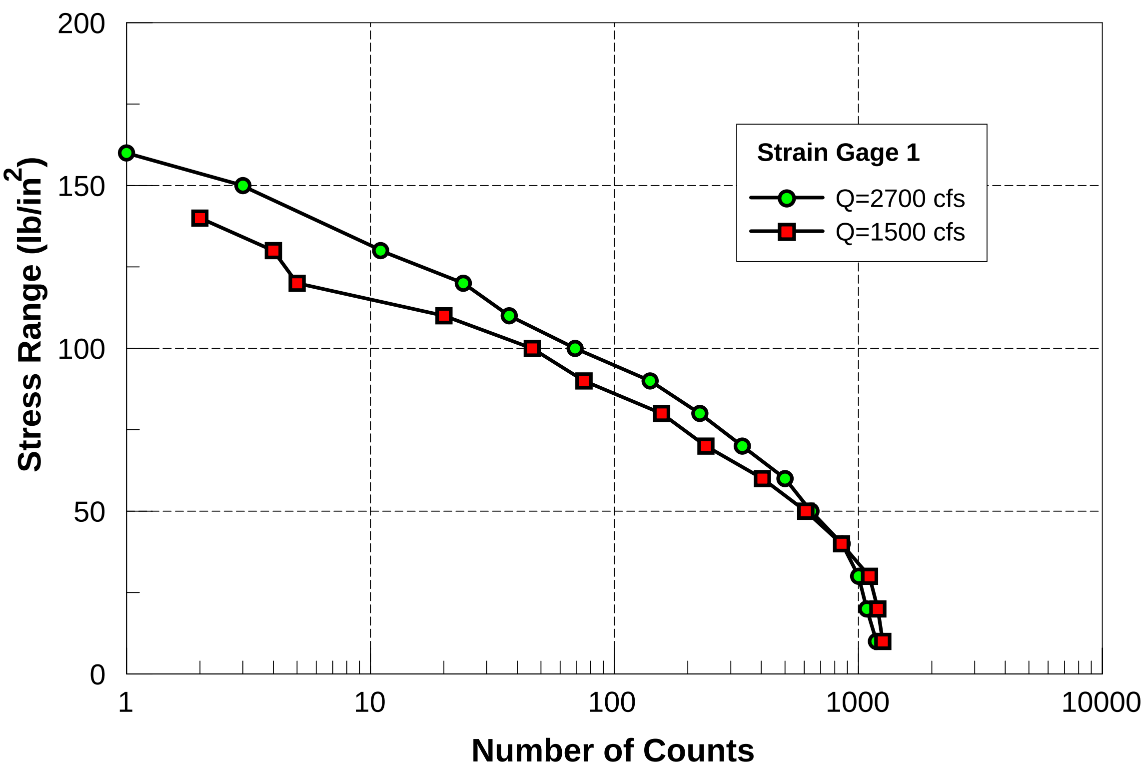

Figure22: Histogram of stress range counts for strain gage 1 for the two discharges.

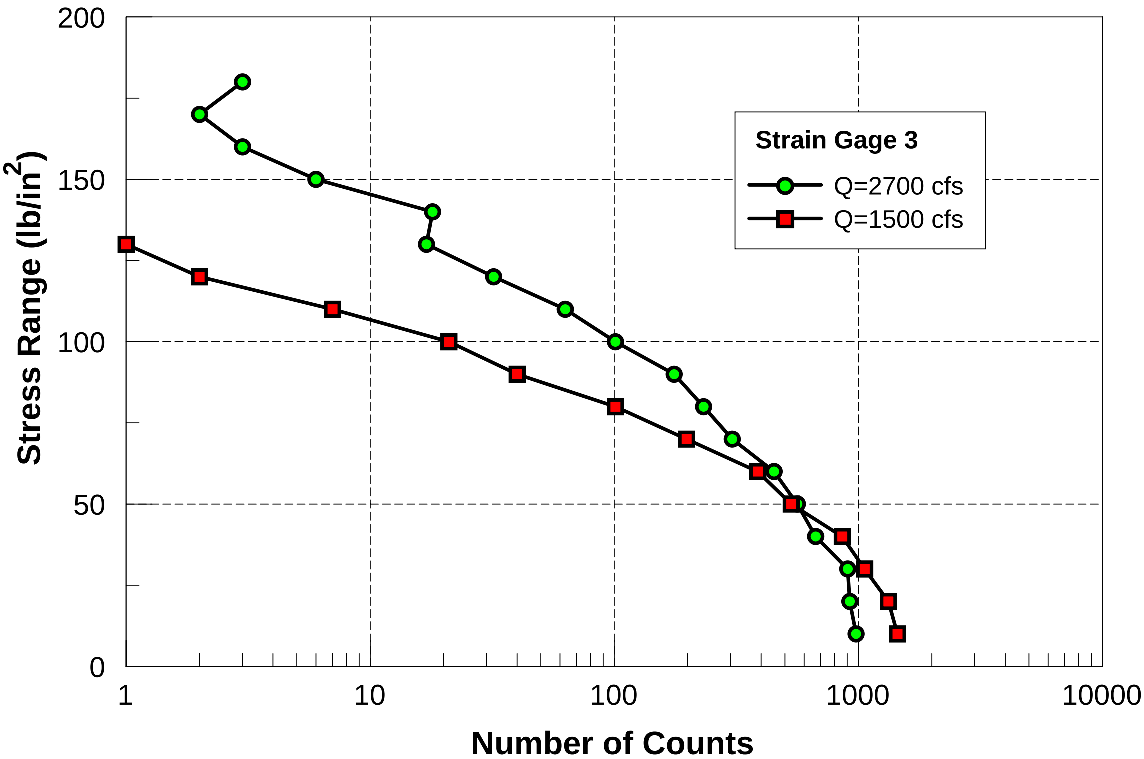

Figure 23: Histogram of stress range counts for strain gage 3 for the two discharges.

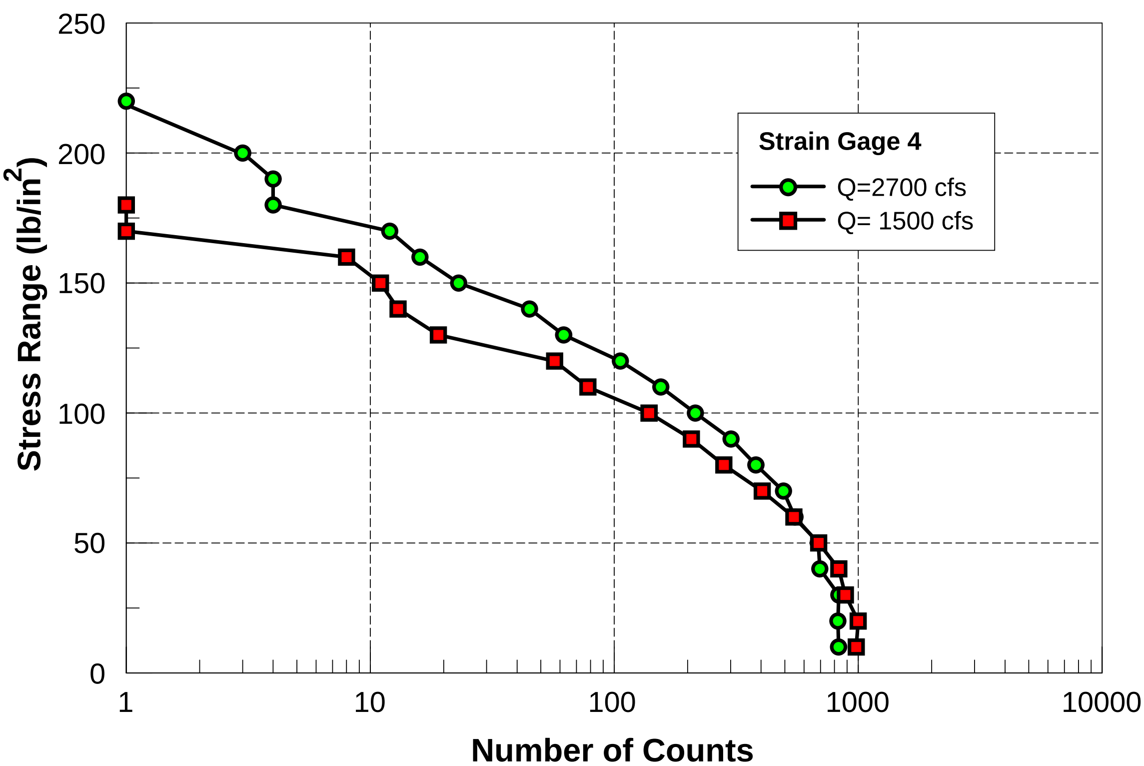

Figure 24: Histogram of stress range counts for strain gage 4 for the two discharges.